Supplementary Information

Copper complexes with dissymmetrically substituted bis(thiosemicarbazone) ligands as a basis for PET radiopharmaceuticals: control of redox potential and lipophilicity

Oliver C Brown,[1§] Julia Baguña Torres,[2§] Katherine B Holt,[3] Philip J Blower[2*] and Michael J Went[*,1]

[1]University of Kent, School of Physical Sciences, Canterbury CT2 7NH, UK

[2]King's College London, Division of Imaging Sciences and Biomedical Engineering, 4th Floor Lambeth Wing, St Thomas' Hospital, London SE1 7EH, UK

[3]University College London, Department of Chemistry, 20 Gordon St, London, WC1H 0AJ, UK

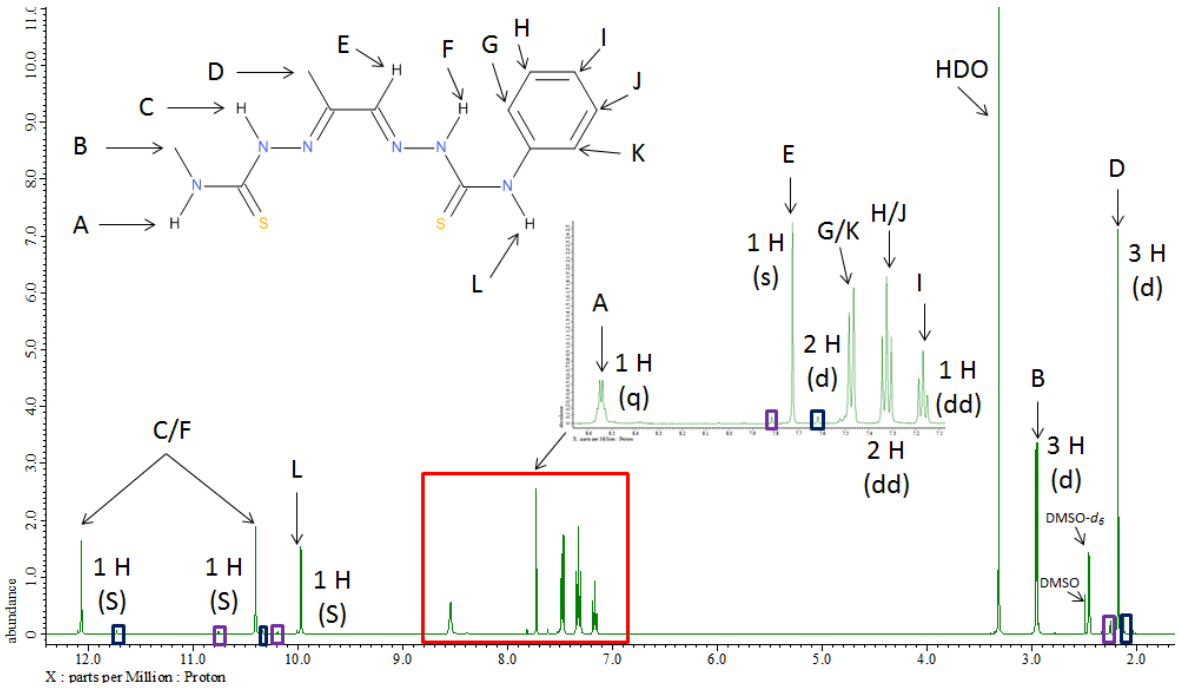

Fig. S1. Assigned ^{1}H NMR spectrum of **12**, successfully synthesised by reacting compound **B** with 4-phenyl-3-thiosemicarabzide. The spectrum suggests a small presence of **8** (purple box) and **5** (Blue box). This is commonly seen in other dissymmetric ligand reactions of this class.

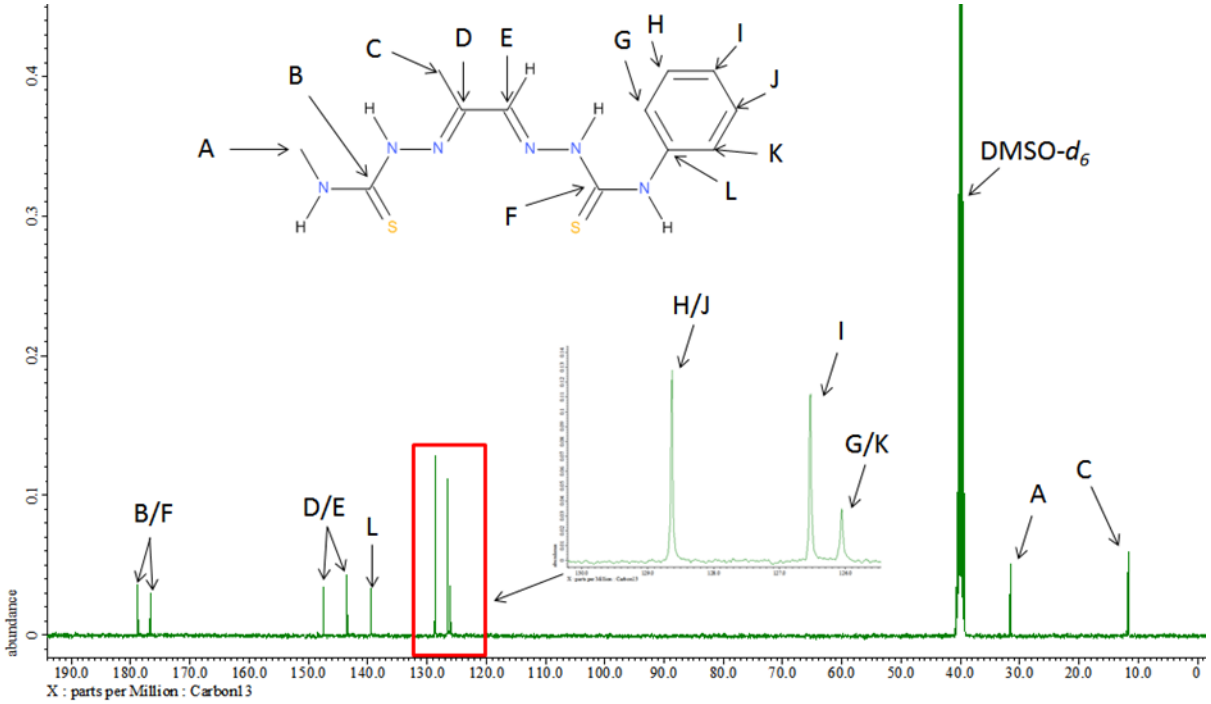

Fig. S2. Assigned ^{13}C NMR spectrum of **12**.

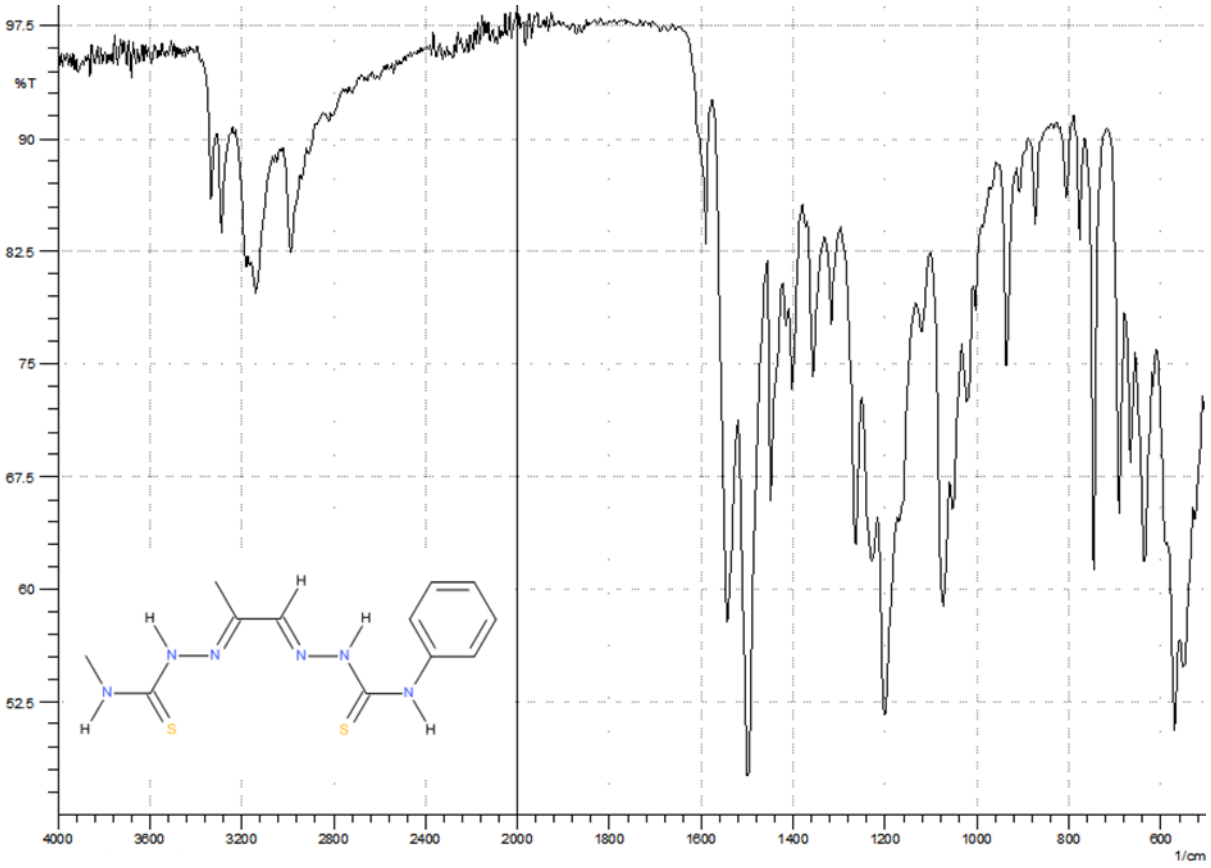

Fig. S3. FTIR spectrum of **12**.

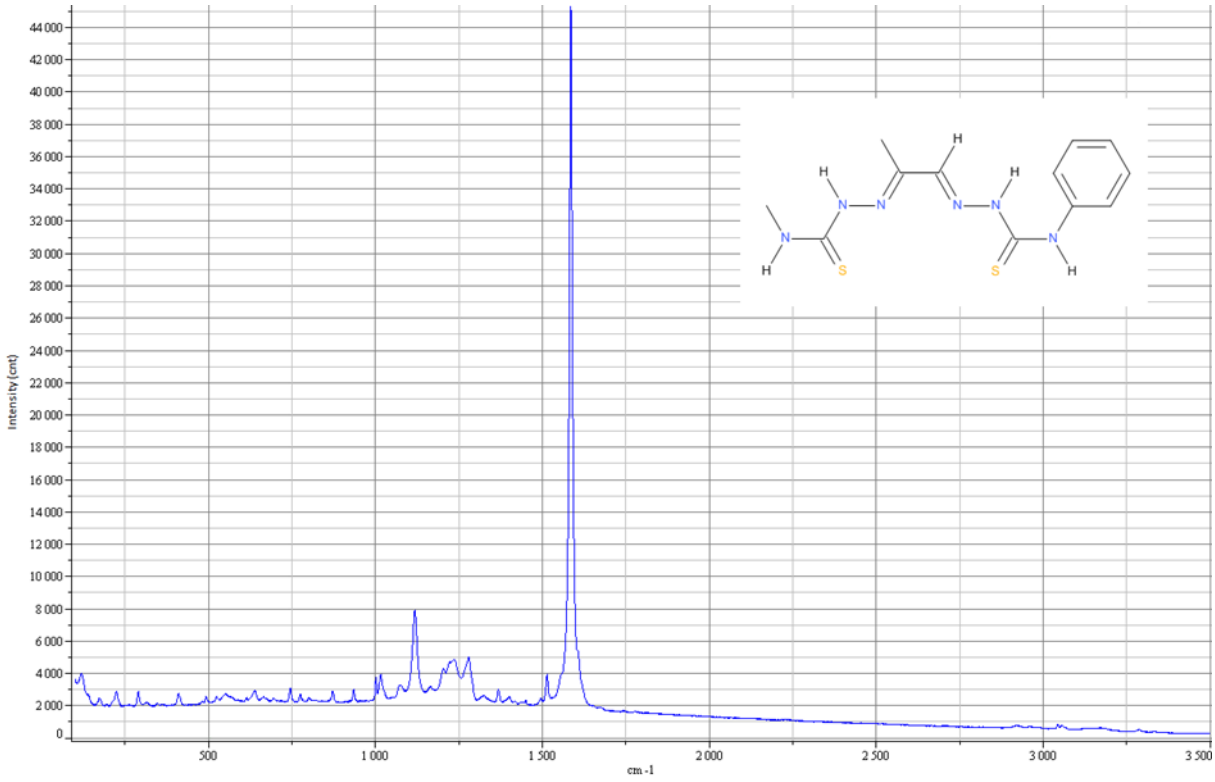

Fig. S4. Raman spectrum of **12**.

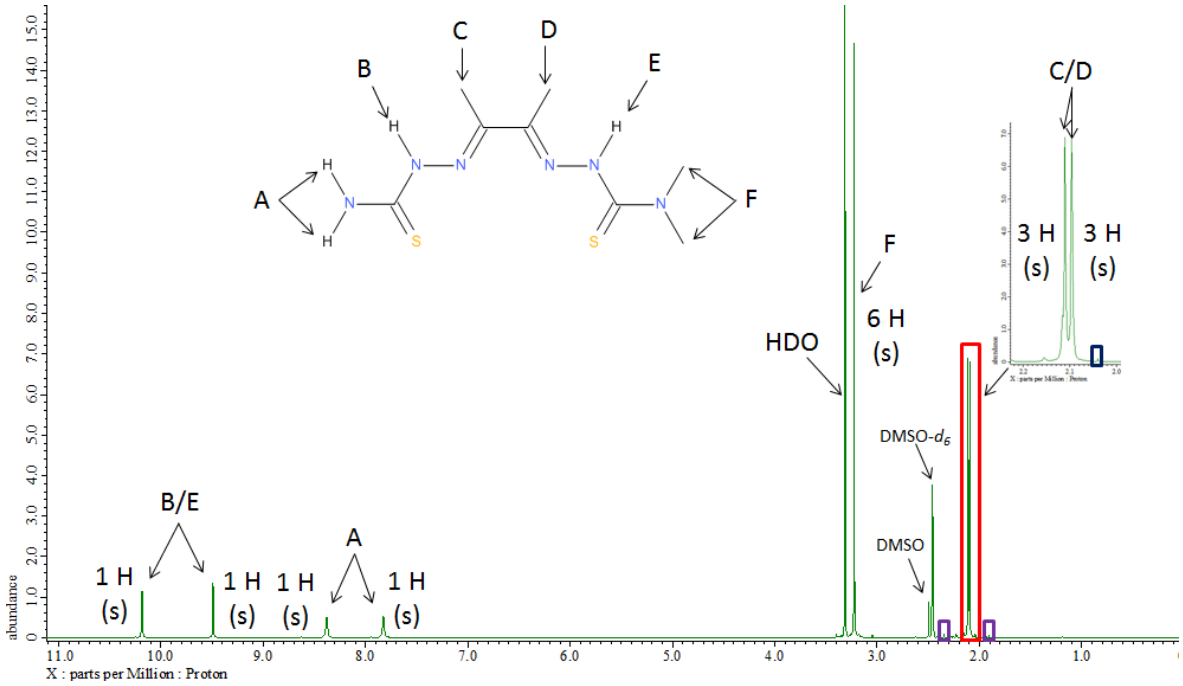

Fig. S5. Assigned ^{1}H NMR spectrum of **24**. This ligand was successfully synthesised by the exploitation of carbonyl reactivity approach by reacting **G** with 4,4-dimethyl-3-thiosemicarbazide. The purple and blue boxes indicate a very small presence of **G** and **33** respectively.

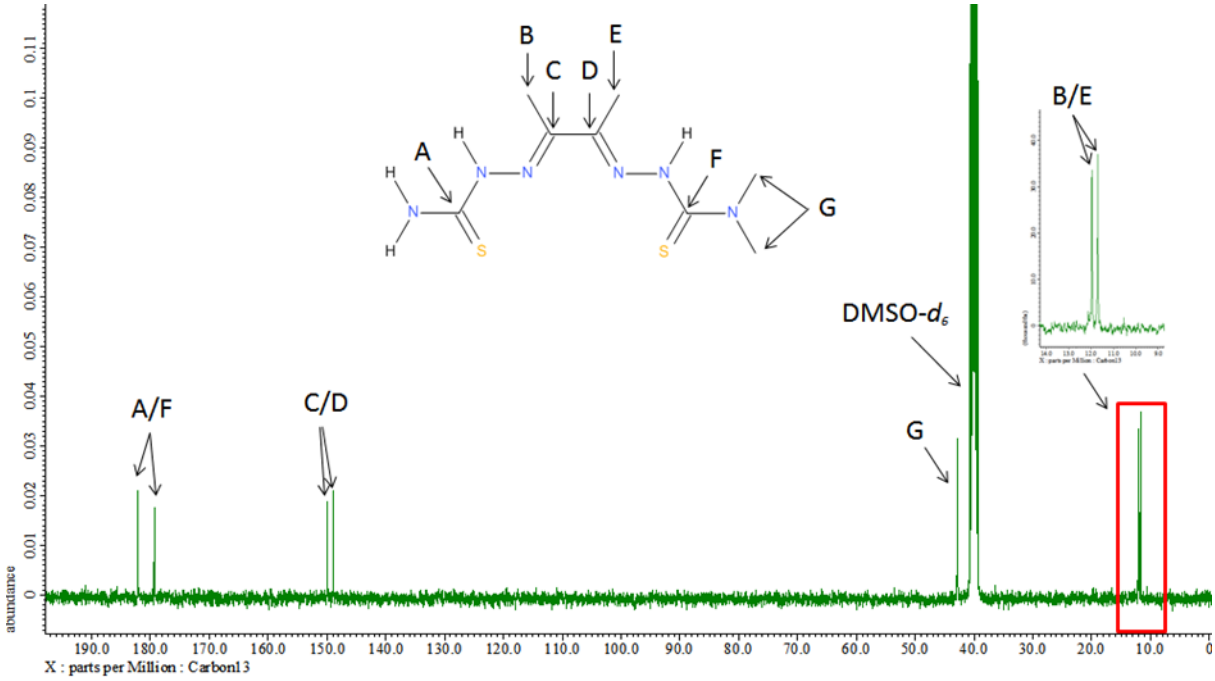

Fig. S6. Assigned ^{13}C NMR spectrum of **24**.

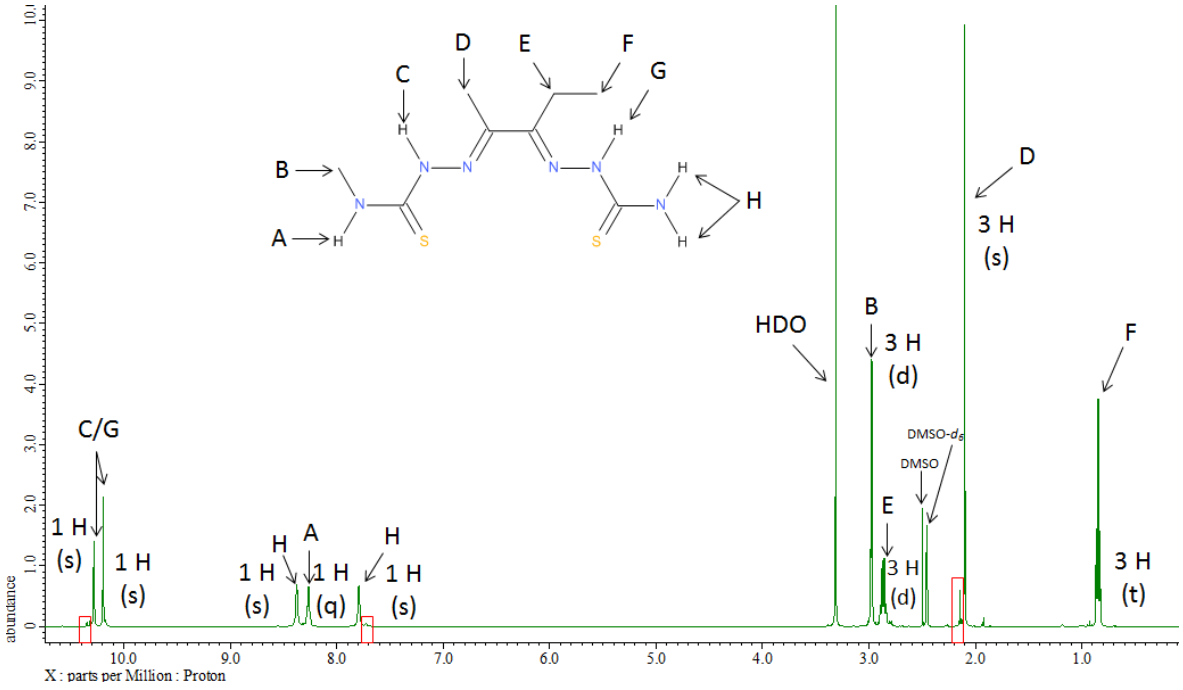

Fig. S7. Assigned ^{1}H NMR spectrum of **29**, which was successfully synthesised by reacting **L** with thiosemicarbazide. The red boxes show a small presence of the "scrambled" isomer **26**.

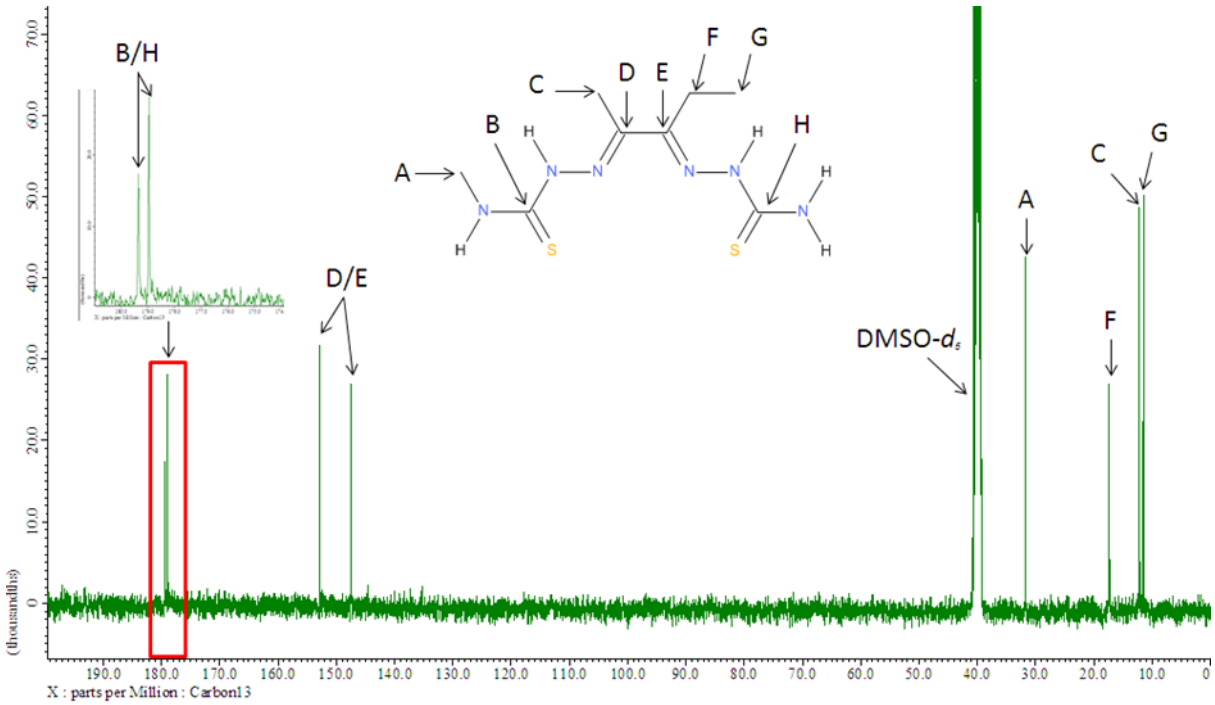

Fig. S8. Assigned ^{13}C NMR spectrum of **29**.

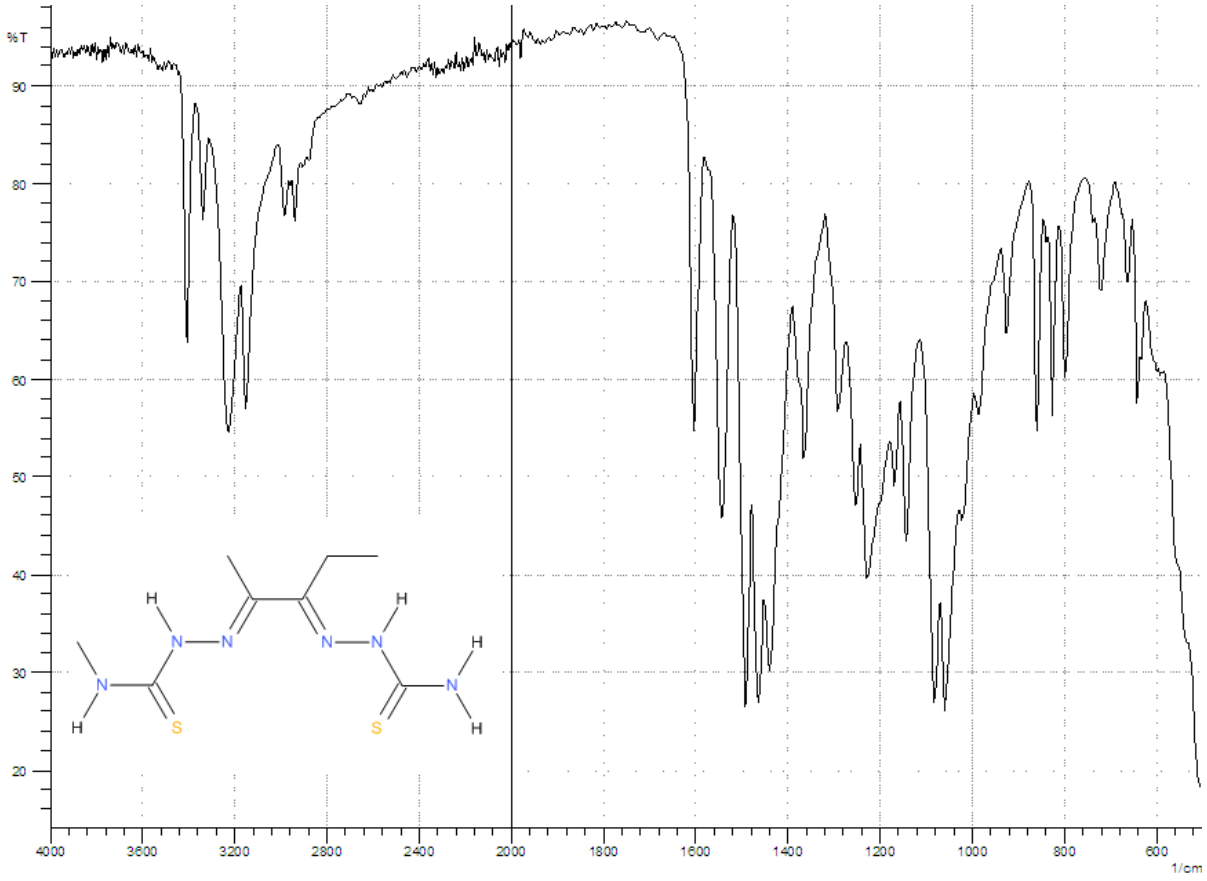

Fig. S9. FTIR spectrum of **29**.

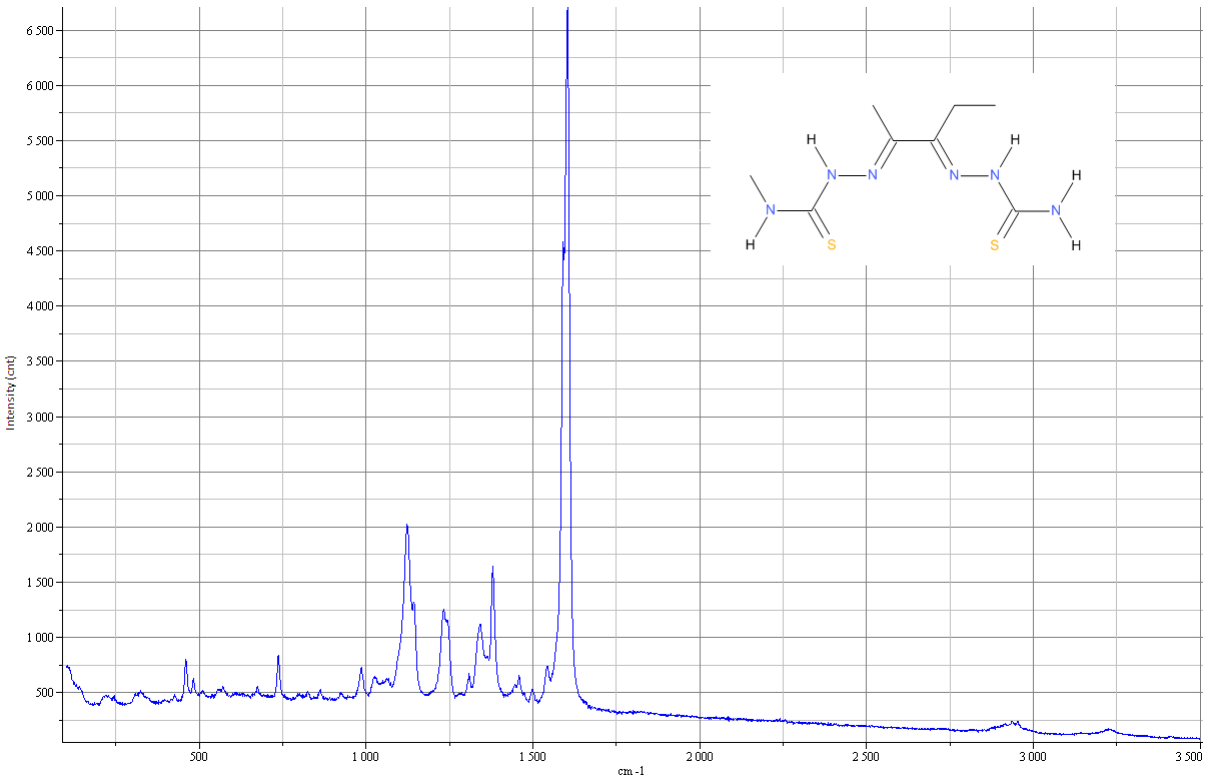

Fig. S10. Raman spectrum of **29**.

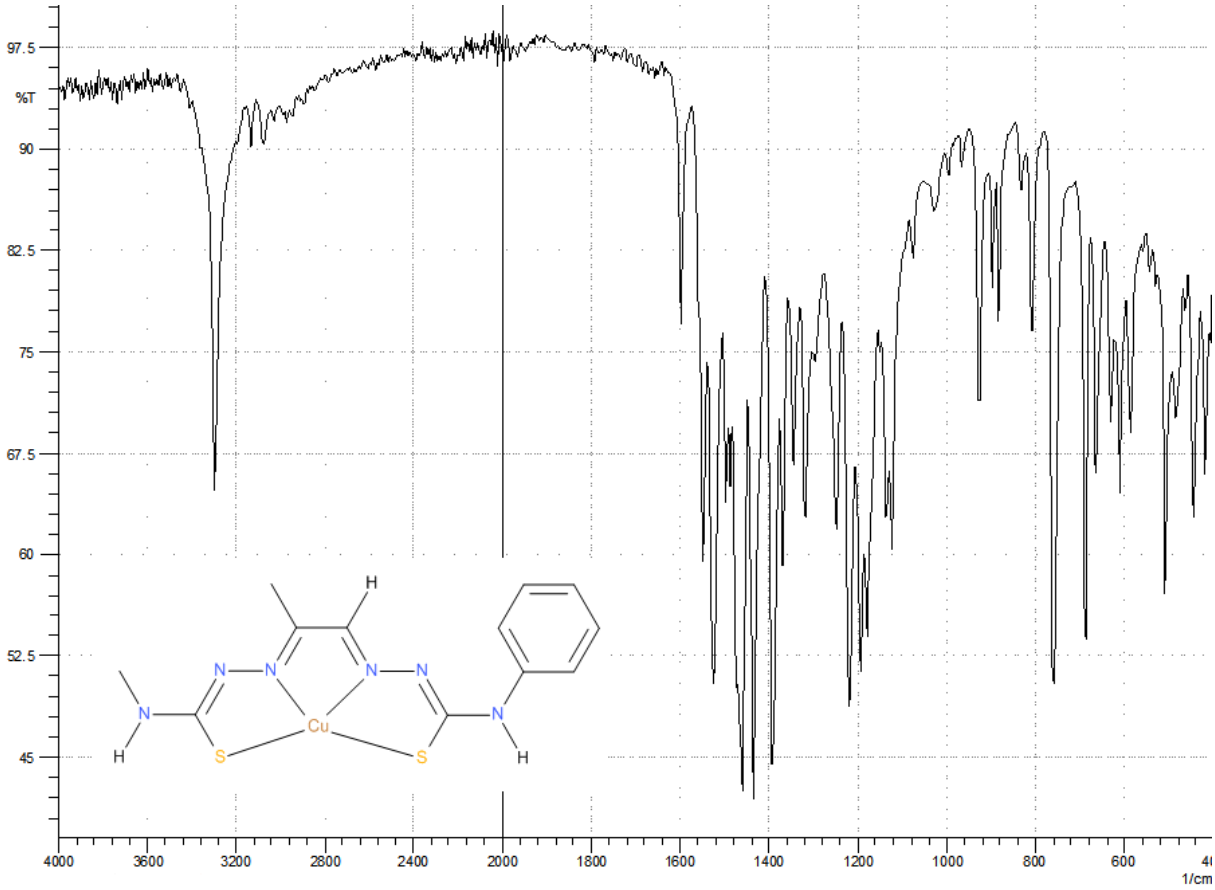

Fig. S11. FTIR spectrum of **Cu(12)**.

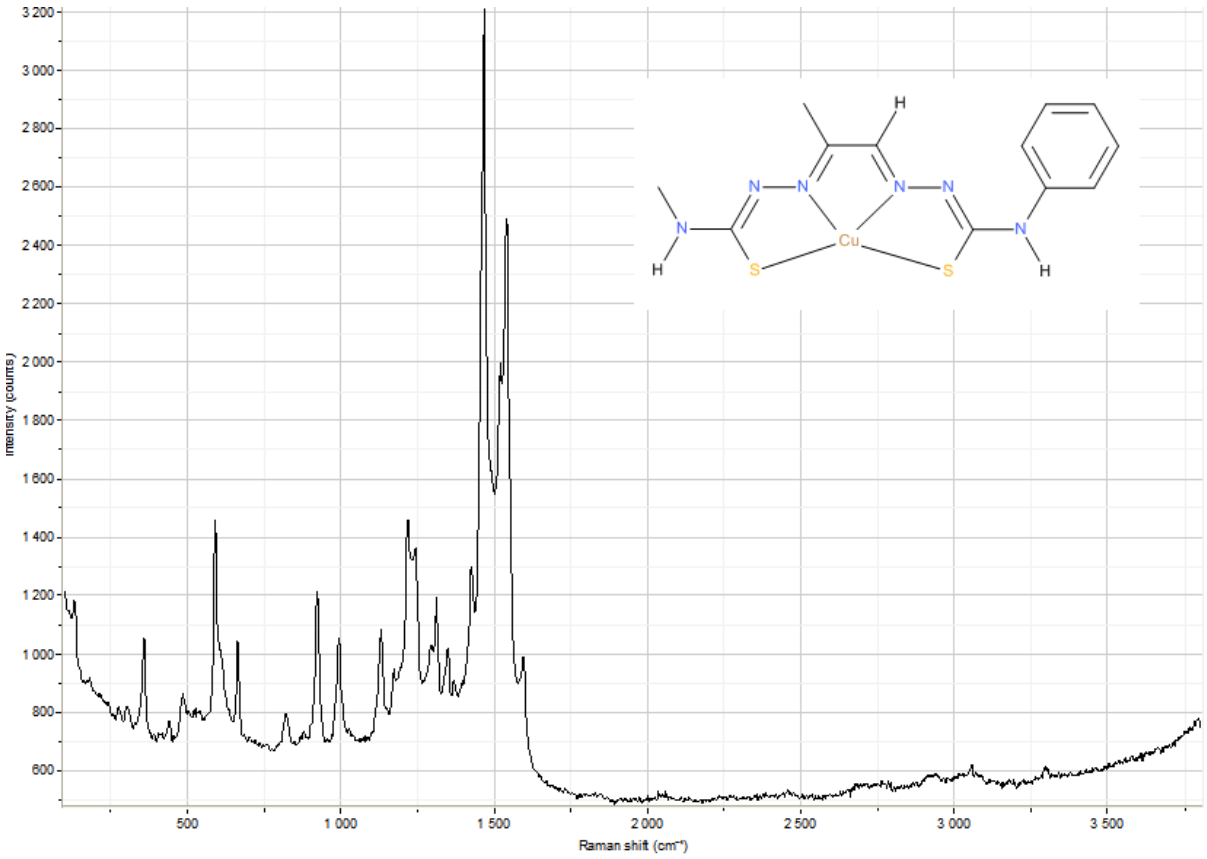

Fig. S12. Raman spectrum of **Cu(12)**.

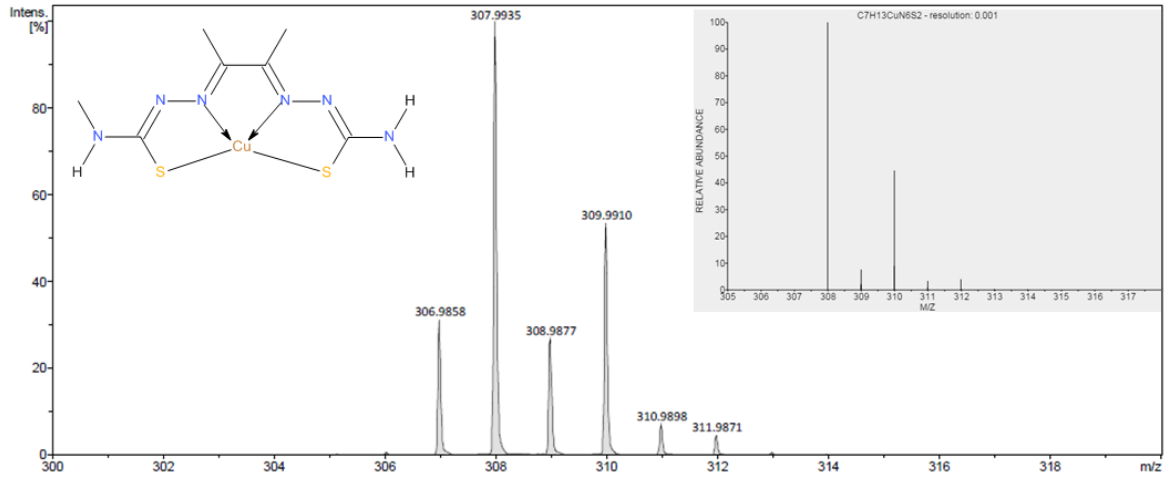

Fig. S13. Mass spectrum of **Cu(23)**. The spectrum in the top right hand corner is the predicted spectrum of the M + H^+ ion of **Cu(23)** generated by ChemCalc.

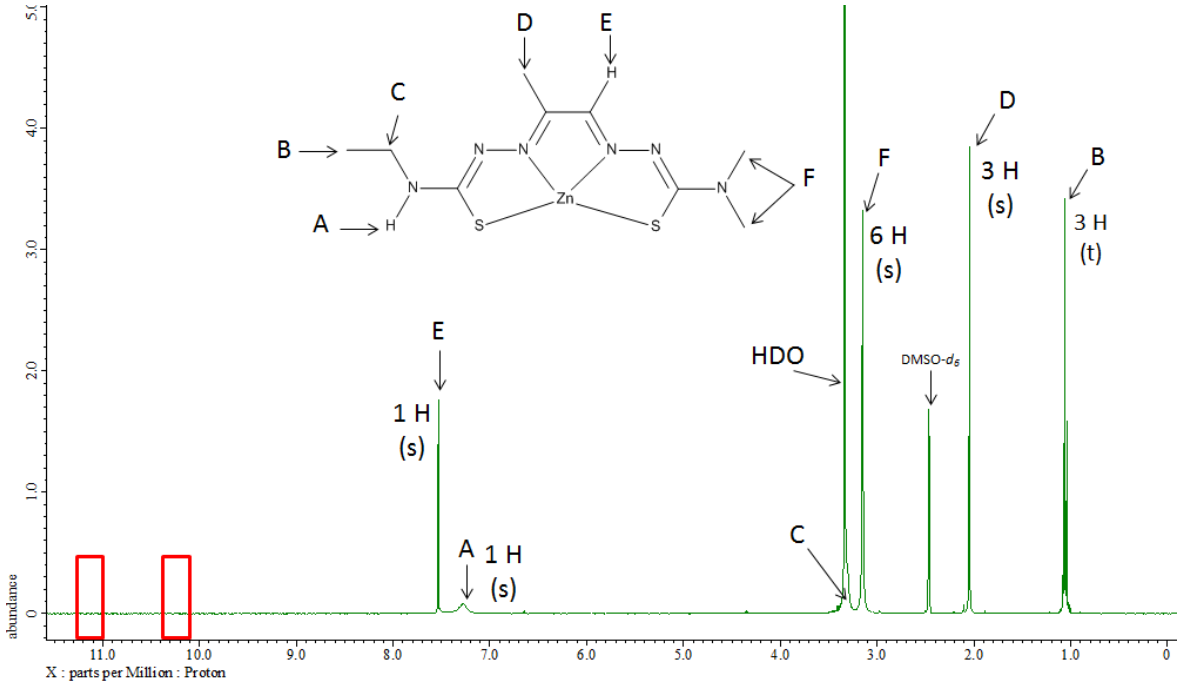

Fig. S14. An assigned proton NMR spectrum of the complex **Zn(14)**. The red boxes illustrates the location of the N-N-H protons would be if there was any **14** ligand present. Environment C is located underneath the water peak, this has been shown with other complexes where a HMQC NMR spectrum has been acquired.

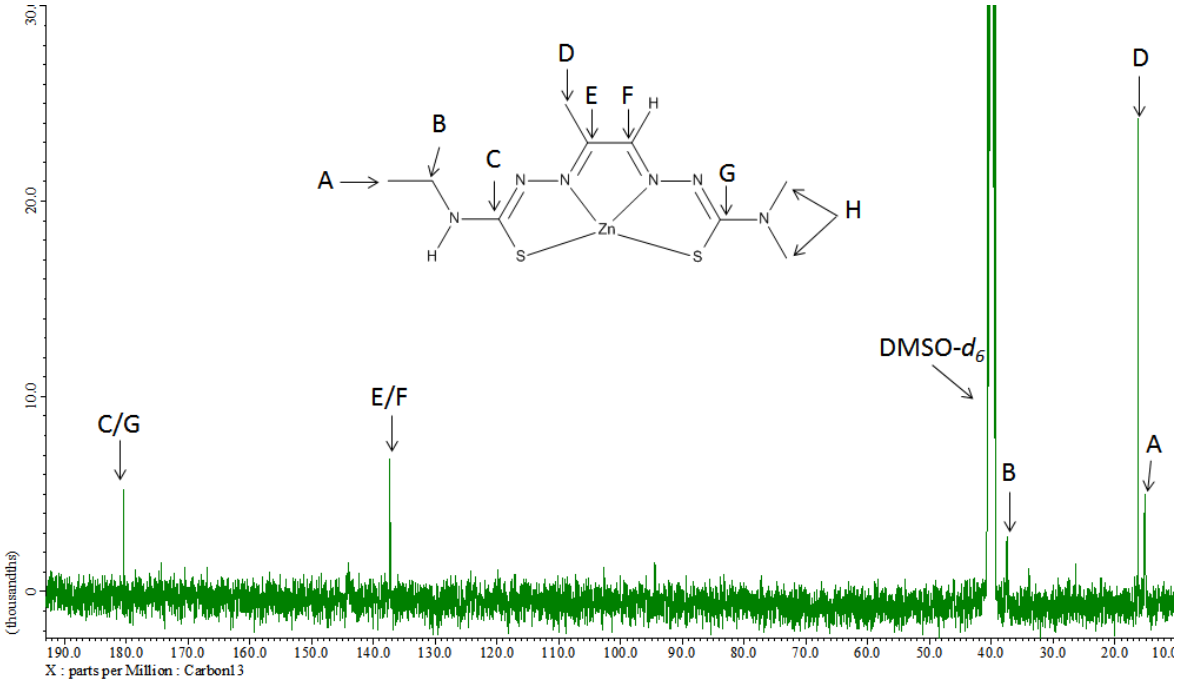

Fig. S15. Assigned carbon NMR spectrum of the complex **Zn(14)**. It is believed that environment H is not visible because the signal is particularly weak. It is unclear if the peaks at 180.44 ppm and 137.31 ppm are both or one of environments C/G and E/F respectively.

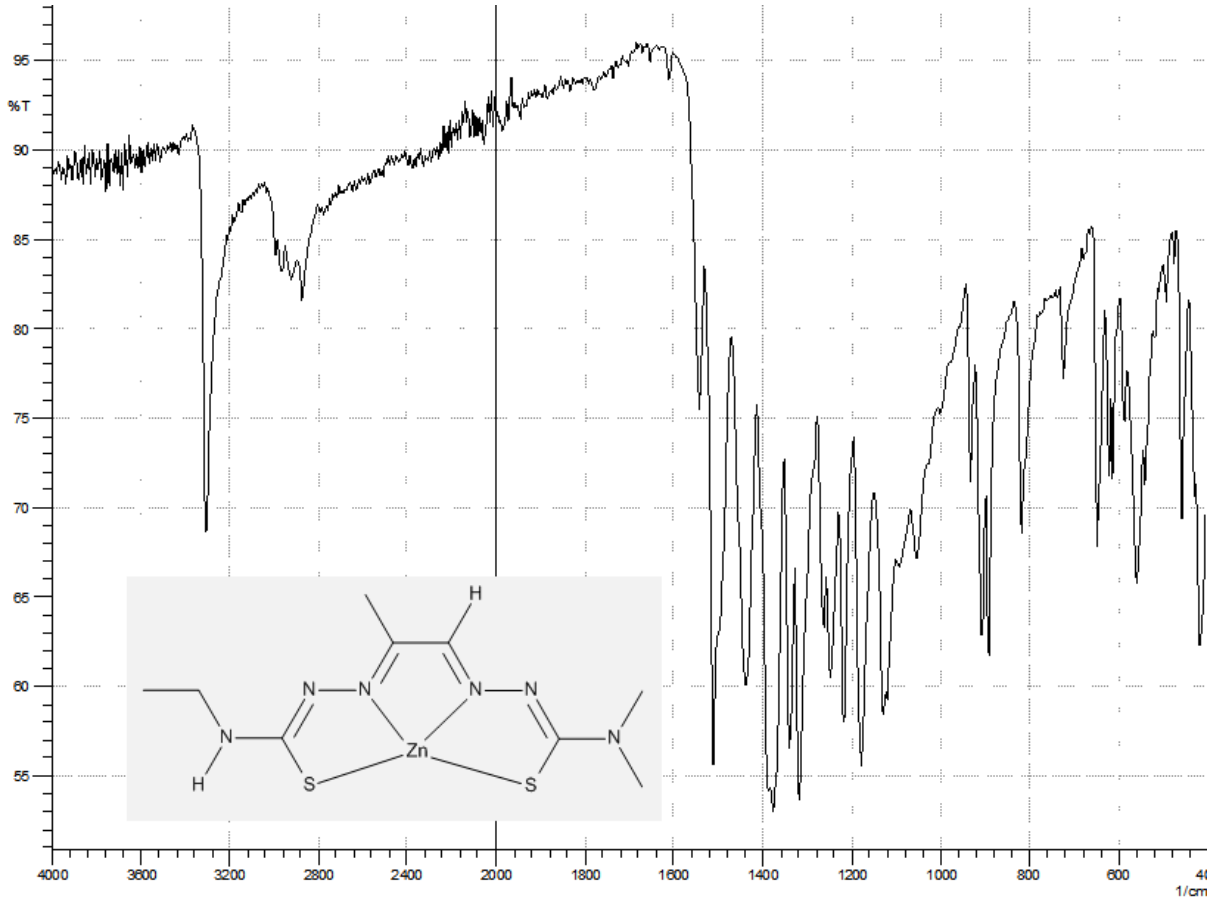

Fig. S16. FTIR spectrum of the complex **Zn(14)**.

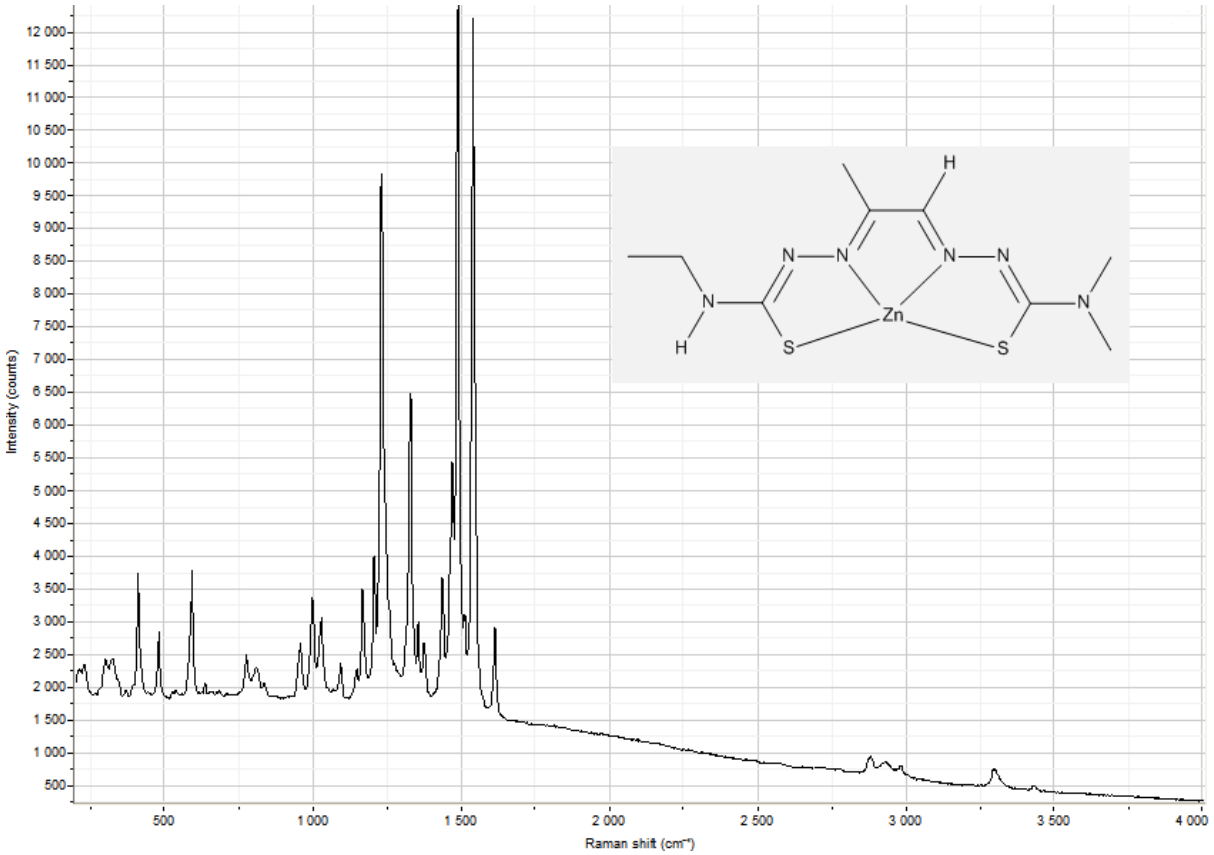

Fig. S17. Raman spectrum of the complex **Zn(14)**.

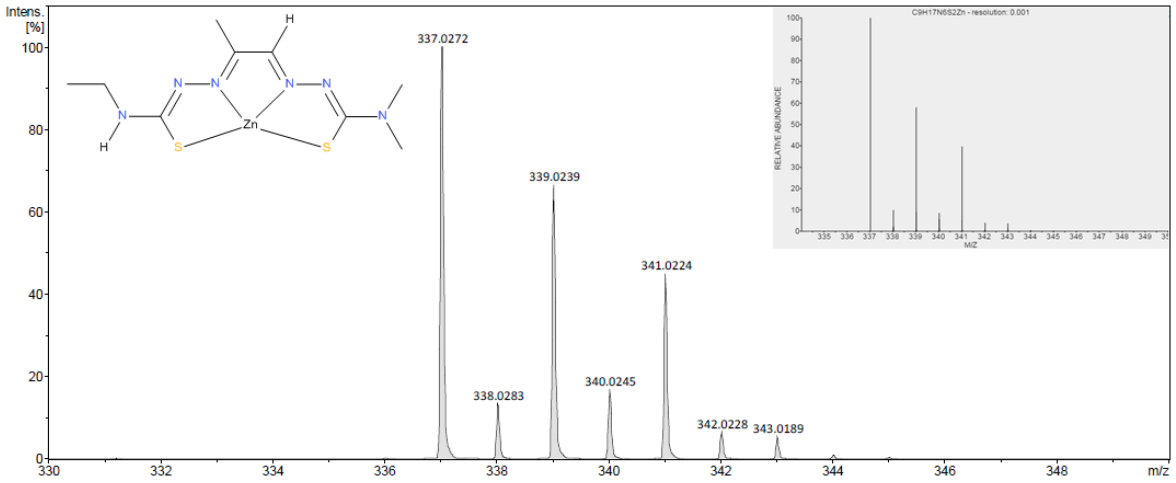

Fig. S18. Mass spectrum of **Zn(14)**. The spectrum in the top right hand corner is the predicted spectrum of the M + H^+ ion of **Zn(14)** generated by ChemCalc.

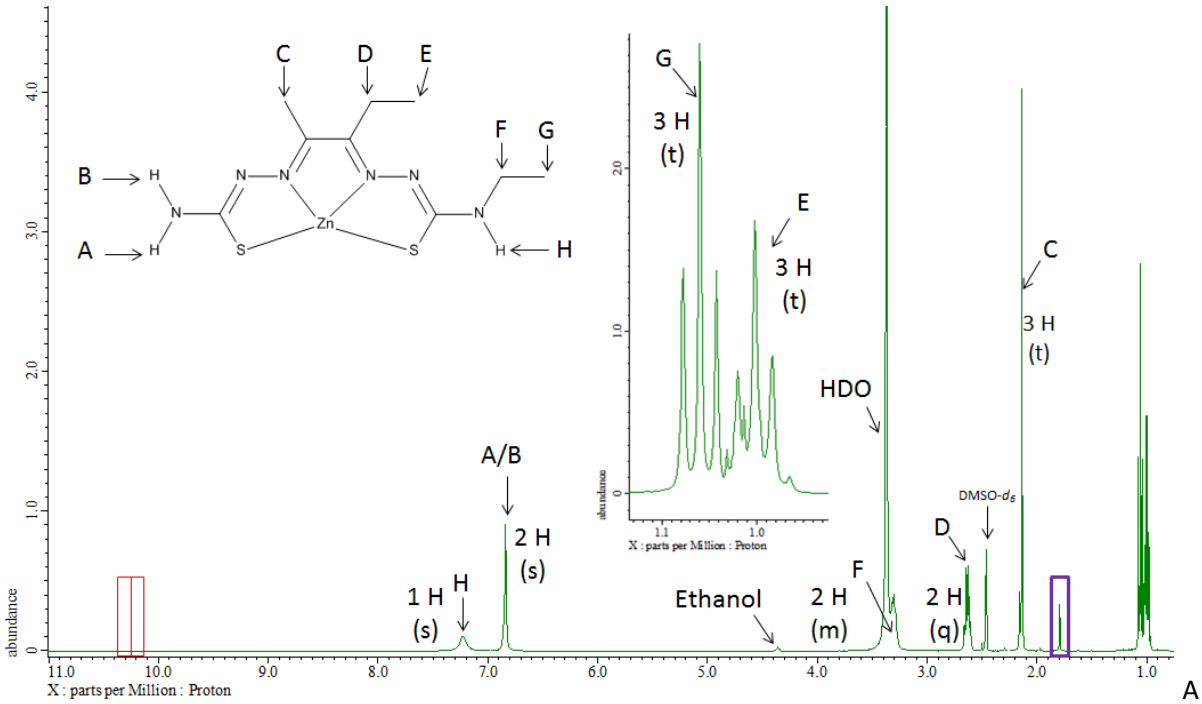

Fig. S19. ^{1}H NMR spectrum of the complex **Zn(28)**. The red boxes illustrates the location of the N-N-**H** protons would be if there was any **28** ligand present. Environment F is overlapped by the water peak, this is has been shown with the HMQC NMR spectrum. The purple box shows this presence of an unassigned peak.

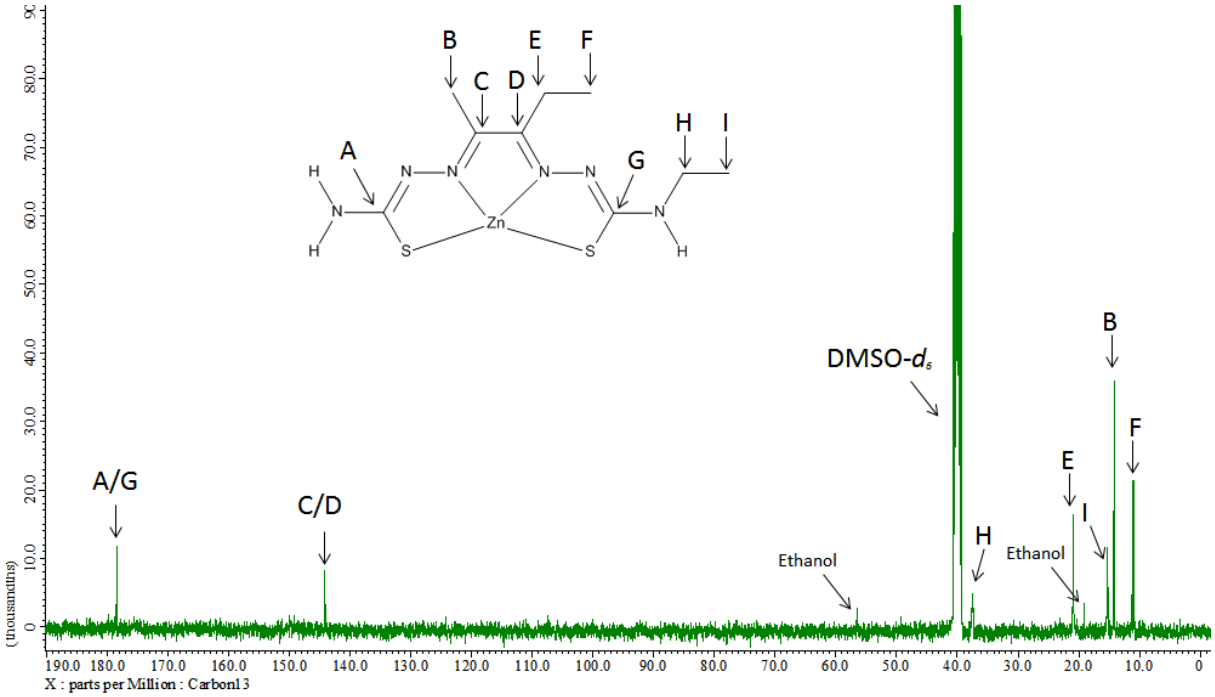

Fig. S20. Assigned carbon NMR spectrum of the complex **Zn(28)**.

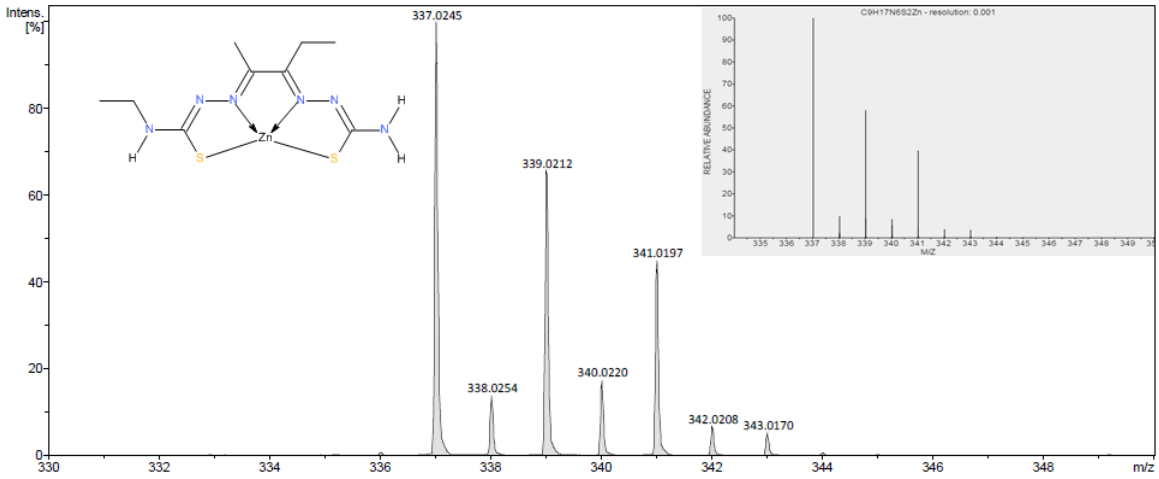

Fig. S21. Mass spectrum of **Zn(30)**. The spectrum in the top right hand corner is the predicted expected spectrum of the M + H^+ ion of **Zn(30)** generated by ChemCalc.

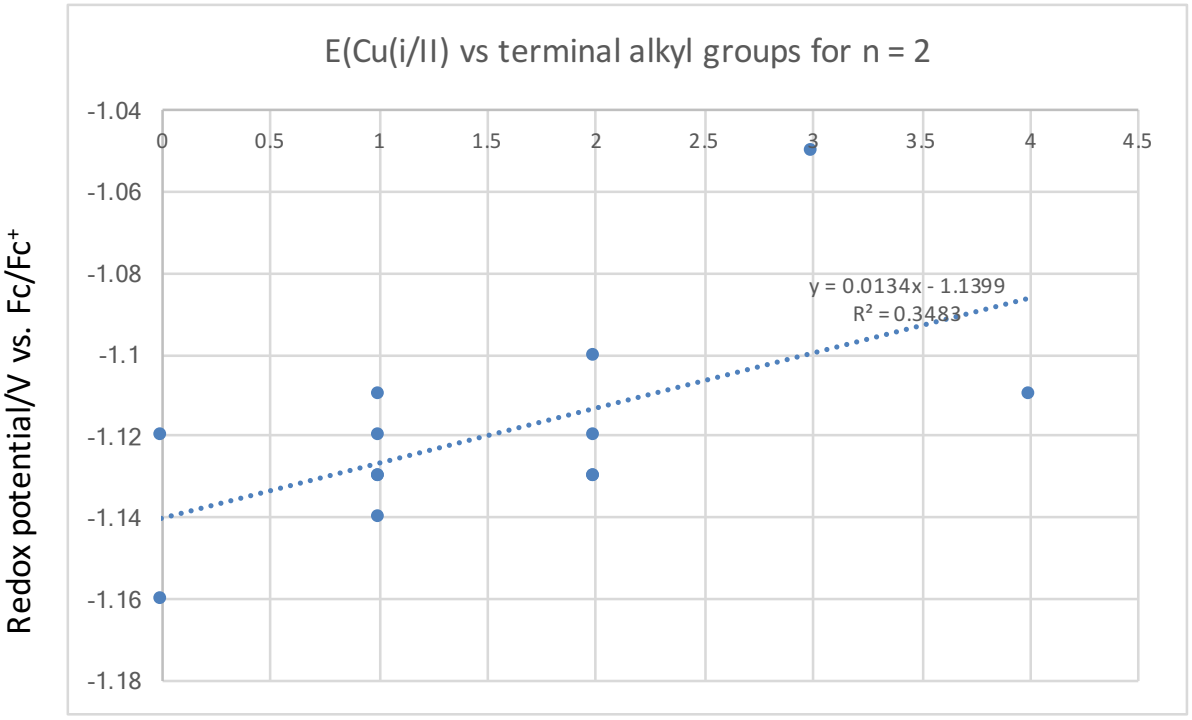

Fig. S22. Correlation, with regression lines, of Cu(I/II) redox potentials with terminal alkylation at R_1 – R_4, including only compounds with two alkyl groups at Q_1/Q_2. Some points have been offset slightly horizontally for visual clarity. All available data are included, from this work and literature data (corrected for different referencing), with the exception of compounds containing phenyl groups.

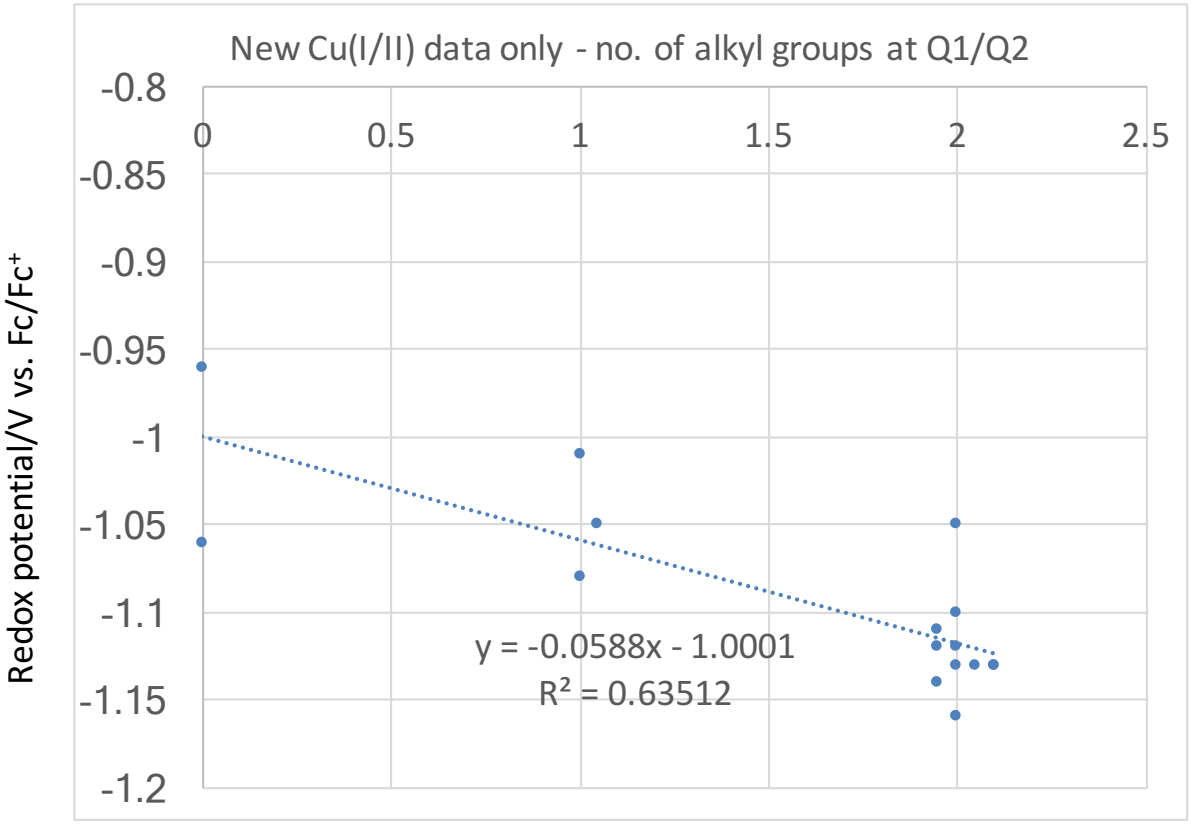

Fig. S23. Correlation, with regression lines, of Cu(I/II) (top) and Cu(II/III) (bottom) redox potentials with alkylation at Q_1 and Q_2. Some points have been offset slightly horizontally for visual clarity. Only new data are included, from this work; compounds containing phenyl groups are excluded.

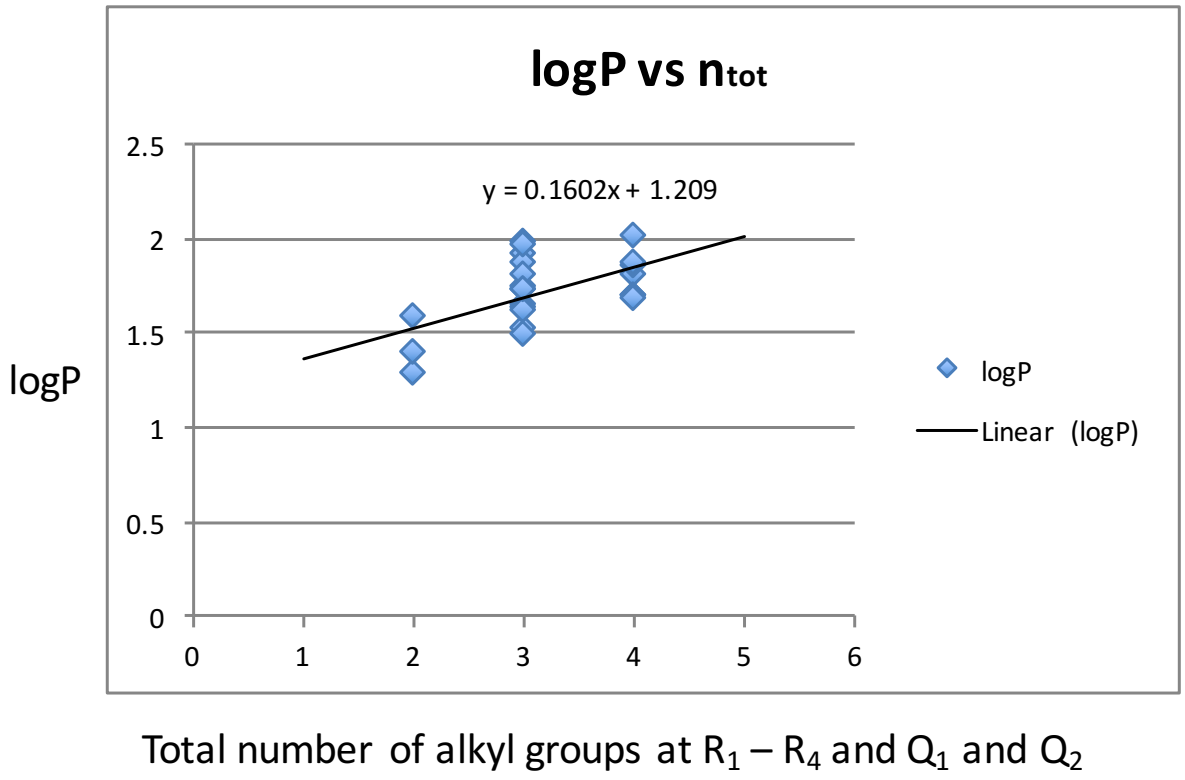

Fig. S24. Plot of logP of copper BTSC complexes against total number of alkyl groups at R1-4 and Q1-2 (n_{tot}). The regression line shows that alkylation increases logP on average by 0.16 per alkyl group, although the location and identity of the alkyl/aryl group also has a significant effect. Values of logP for copper complexes with n<2 and n>4 were not determined.